

# Electronic Counter-Countermeasure Capabilities of Chaos-Based FM Radar

Justin Gold

ECE-499: Electrical and Computer Engineering Capstone

Advisor: Professor Chandra S. Pappu

March 26, 2020

# Contents

<b>1</b>	<b>Report Summary</b> . . . . .	<b>5</b>
<b>2</b>	<b>Introduction</b> . . . . .	<b>5</b>
<b>3</b>	<b>Background</b> . . . . .	<b>7</b>
<b>4</b>	<b>Components of Project Design</b> . . . . .	<b>8</b>
4.1	The Transmitted Signal . . . . .	8
4.2	The Received Signal . . . . .	10
4.3	The Linear FM Waveform . . . . .	11
4.4	The Chaos-Based FM Waveform . . . . .	12
<b>5</b>	<b>Preliminary Methodology</b> . . . . .	<b>12</b>
5.1	The Chaotic Systems . . . . .	12
5.2	Compression Factors . . . . .	14
5.3	Generating the Transmitted Waveforms . . . . .	14
<b>6</b>	<b>Characteristics of CBFM Waveforms</b> . . . . .	<b>15</b>
6.1	The FM Waveforms in the Frequency Domain . . . . .	15
6.2	Autocorrelations . . . . .	16
<b>7</b>	<b>Implementation of a Smart Jammer</b> . . . . .	<b>18</b>
<b>8</b>	<b>Implementation of High-Resolution Imaging</b> . . . . .	<b>23</b>
8.1	Ambiguity Functions . . . . .	24
8.2	Signature Analysis . . . . .	25
8.3	Signature Analysis with Noise . . . . .	27
8.4	Entropy Analysis . . . . .	29
<b>9</b>	<b>Performance Estimates and Results</b> . . . . .	<b>29</b>

9.1	Signature Analysis Results . . . . .	29
9.2	Entropy Analysis Results . . . . .	31
<b>10</b>	<b>Discussion, Conclusion, and Recommendations . . . . .</b>	<b>32</b>
10.1	Lessons Learned . . . . .	33
<b>11</b>	<b>References . . . . .</b>	<b>34</b>

## List of Figures

1	Total Distance from Radar to Target Block Diagram . . . . .	10
2	Voltage of x-state variables over time for each chaotic system . . . . .	15
3	Power Spectrums of the CBFM Signals over 100 Monte-Carlo Simulations . . . . .	16
4	Sidelobe levels from Autocorrelations of CBFM Waveforms . . . . .	17
5	Mainlobes of waveforms at -3dB . . . . .	18
6	I/Q Detector Block Diagram . . . . .	19
7	Jammer Extracted $h_I(t)$ and $h_Q(t)$ Components of ACT System . . . . .	20
8	Jammer Extracted $I(t)$ and $Q(t)$ Components of ACT System . . . . .	20
9	RMSE Between Actual and Recovered Instantaneous Frequency . . . . .	22
10	Actual and Recovered Instantaneous Frequency at $K=0.5$ . . . . .	22
11	X and Y Dimensions of Complex Target . . . . .	23
12	Results of the Ambiguity Function with Time $\tau = 0$ s and $f_D = 0$ Hz . . . . .	25
13	Block Diagram of Signature Analysis . . . . .	27
14	Signature Analysis Results with SNR = 0dB . . . . .	30
15	ACT Signature Analysis with SNR = -5dB, -10dB, -15dB, -20dB . . . . .	31
16	Entropy Analysis of Waveforms at SNR levels from -40 dB to 0dB . . . . .	31

## List of Tables

1	Initial Conditions for Generating Chaotic Waveforms . . . . .	14
2	Finalized Compression Factors . . . . .	14

# 1 Report Summary

This project examined the capabilities of electronic counter-countermeasures and high-resolution imaging of a chaos-based FM radar. Four chaotic systems, the Moore-Spiegel system, the Lorenz system, the ACT system, and the Rossler system were used in simulations as transmitted radar signals. Characteristics for each of the signals were considered, including the power spectrums and the autocorrelations. To demonstrate the chaos-based FM waveforms' electronic counter-countermeasure capabilities, a smart jammer was implemented and each of the CBFM waveform's ability to counteract the jammer was observed. To assess the high-resolution imaging capabilities of each chaotic system, the ambiguity function, signature analysis with various noise levels, and entropy analysis were implemented. It was observed that chaos-based FM signals can be used to counteract a jammer by increasing the bandwidth of the signals, and that each chaotic system was capable of generating high-resolution images of a complex target.

## 2 Introduction

Radar, which stands for radio detection and ranging, has played a fundamental role in modern technology. It has been implemented in various applications such as the military, climate monitoring, traffic surveillance, and self-driving cars. An essential application in a military setting is high-resolution imaging of a target. For the radar to generate a high-resolution image of the target, multiple points of the target in close proximity must be distinguishable from each other, and none of the points should be overlapping [13]. A significant determinant of the high-resolution capabilities of a radar lies in the properties of the signal that is transmitted. To increase the resolution, small pulse duration and a high bandwidth are required [13]. For this reason, FM signals are used in radar as they possess higher bandwidths compared to other forms of modulation, such as amplitude-modulated waveforms. Because chaotic systems possess noise-like behavior, and in turn, possess high bandwidths, there has been a high level of interest in implementing chaotic systems in recent radar research [1].

A significant issue found in a monostatic radar, a configuration where the transmitter and receiver are collocated, is that it is vulnerable to jamming, or electronic countermeasures [17]. In the case of a smart jammer, the jammer can demodulate a transmitted signal to attain an estimate of the instantaneous frequency of the transmitted signal [8]. It can then recreate the FM signal using the demodulated signal as instantaneous frequency. In the presence of a jammer system, the radar will assume that the signal was reflected off of a target, thereby creating a false alarm. To prevent the jammer from impacting the performance of the radar, a signal in which a jammer is unable to accurately recover its instantaneous frequency is required. With the introduction of a chaos-based waveform, it is hypothesized that the jammer may be counteracted due to the high bandwidth of a chaotic waveform. Thus, the primary objective of this project is to examine the ability of a chaos-based radar to counteract a jammer, or to observe the chaotic radar's electronic counter-countermeasure (ECCM) capabilities.

Another objective is to determine whether it would be possible for the use of chaotic systems in a monostatic radar setting to generate high-resolution images of a target. If the chaotic systems are capable of counteracting a jammer but were not capable of high-resolution imaging, the systems would be ineffective.

The remainder of the report is divided as following: the background describes the previous research of chaotic systems in radar, as well as any potential societal impact the results of the project could cause. Then, the components of the project design are discussed. The mathematical representation of a transmitted radar waveform and a received radar waveform are provided. The most commonly used waveform in modern radar, the linear FM waveform, is discussed. It is compared to the focus of this project, the chaos-based FM waveform. The preliminary methodology discusses the properties of the chaotic systems used in this project, and how FM waveforms were generated using chaotic systems. The section called characteristics of CBFM waveforms described the initial signal processing techniques conducted on each CBFM waveform, and how they are used to hypothesize results of performance in high-resolution imaging and its ECCM capabilities. Then,

the implementation of a smart jammer and the implementation of high-resolution imaging are discussed. The results of these tests are discussed in the performance estimates and results section. Finally, conclusions are drawn in the discussion, conclusion, and recommendations section.

### **3 Background**

The use of discrete chaotic maps and continuous chaotic waveforms as FM signals have gained attention in recent radar research. The idea and application of discrete chaotic signals in radar systems was introduced in [3] and [2]. Following this, discrete chaotic maps such as the Bernoulli, Tent, Logistic, and Quadratic discrete maps were analyzed. Through various simulations including autocorrelations, the ambiguity function, and entropy analysis of each discrete waveform, it was proved that chaotic signals are desirable for high-resolution radar imaging [6]. Much work has also been studied on continuous CBFM waveforms. Wideband FM signals were created with the Lorenz chaotic system as the signal's instantaneous frequency. Time autocorrelations displayed that the FM signal using the Lorenz chaotic system has high range resolution for zero Doppler shift [7]. Other research has compared the spectral properties of FM signals using the Lorenz chaotic system and the Lang-Kobayashi chaotic system [5]. It was found that the spectrums of these signals followed Woodward's theorem in that the shape of the spectrum of a random FM signal resembled the shape of the probability density function of the instantaneous frequency of the signal. It was also found that the signals were candidates for high resolution imaging and that the achievable range resolution is higher for continuous chaotic systems than signals generated from discrete maps. It was left as a question to whether CBFM waveforms could have potential in anti-jamming [5].

The societal impact this will make is that it furthers the research of chaotic radar. If implemented, it could greatly reduce the cost of radar as the cost to ensure the linearity of a transmitted waveform is unnecessary with chaos [10]. The results may impact future radar research and design if it can be shown that chaotic waveforms are able to evade a jammer. In terms of ethics, there is little

negative that could result from this project. In general, the radar system emits electromagnetic radiation which has negative effects on the environment. Radars are also capable of generating electromagnetic interference to other electronic equipment in a close vicinity [4]. This could be harmful to other systems if the radar were to act as an unintentional jammer for nearby technology.

## 4 Components of Project Design

### 4.1 The Transmitted Signal

The first component of the project was designing a transmitted radar waveform. The most basic component of the transmitted FM waveform is a baseband sinusoidal waveform given as [13]:

$$s(t) = A(t)\cos(\theta(t)) \quad (1)$$

The generalized angle of the waveform over time is given by  $\theta(t)$ , and the amplitude is given by  $A(t)$ . For FM signals,  $A(t)$  is kept at a constant value over time. The generalized angle is given as:

$$\theta(t) = 2\pi f_c t + \phi(t) \quad (2)$$

Here,  $f_c$  is the carrier frequency and  $\phi(t)$  is the instantaneous phase. The carrier frequency is to move the signal to a different frequency band. For each of the simulations conducted the carrier frequency was assumed to be 200 MHz. Considering a baseband signal where  $f_c = 0$ , the resulting waveform is expressed as:

$$s(t) = A\cos(\phi(t)) \quad (3)$$

In FM, the frequency of the waveform is determined by the waveform's instantaneous frequency which is given as the derivative of the generalized angle. For a baseband signal the instan-

taneous angular frequency,  $w_i(t)$  is given as:

$$\begin{aligned}w_i(t) &= \frac{d\theta}{dt} \\w_i(t) &= \frac{d(\phi(t))}{dt}\end{aligned}\tag{4}$$

The instantaneous angular frequency and the instantaneous frequency are related by  $w_i = 2\pi f_i$ , and thus the instantaneous frequency is given as:

$$f_i(t) = \frac{1}{2\pi} \frac{d(\phi(t))}{dt}\tag{5}$$

The instantaneous phase can then be written in terms of the instantaneous frequency,  $\phi(t)$ , as shown below:

$$\phi(t) = 2\pi \int_0^t f_i(\lambda) d\lambda\tag{6}$$

The relationship between the instantaneous phase is the basis for generating FM waveforms. In the FM waveform, the instantaneous frequency is proportional to the modulating waveform [11],  $x(t)$ , as shown in Equation (7).

$$f_i(t) = Kx(t)\tag{7}$$

Where  $K$  is a modulation index of the signal. The modulation index is essential in determining the bandwidth of the signal. By increasing the modulation index, the bandwidth of the signal is increased. By substituting the instantaneous frequency in Equation (6), the instantaneous phase is expressed as:

$$\phi(t) = 2\pi K \int_0^t x(\lambda) d\lambda\tag{8}$$

Finally, an FM waveform can be expressed as:

$$s_{FM}(t) = A \cos(2\pi K \int_0^t x(\lambda) d\lambda) \quad (9)$$

## 4.2 The Received Signal

The above-generated FM waveform can be efficiently transmitted for tracking the target. In the presence of the target, the transmitted waveform is reflected back to the receiver. It is assumed that the received signal is an attenuated  $\alpha$ , time delayed  $\tau$ , and Doppler frequency shifted  $f_D$  replica of the transmitted waveform. Mathematically it is expressed as (10). The delay in time is due to the time the waveform takes to travel from the radar towards the target and back to the receiver. The shift in Doppler frequency is due to the movement of the target [16]. The received signal is given as:

$$r(t) = \alpha s(t - \tau) e^{j2\pi f_D t} \quad (10)$$

For simplicity, the received waveform is assumed to have an attenuation factor  $\alpha = 1$ . Figure 1 shows an illustration of the relationship between the distance of a target and the time it takes for the received signal to return to the receiver.

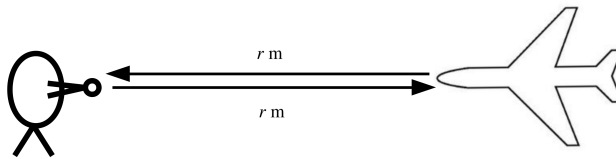


Figure 1: Total Distance from Radar to Target Block Diagram

Assuming that the target is at a range  $r$  meters from the transmitter, the signal must propagate a distance of  $r$  meters and reflect back a distance of  $r$  meters. Note that the FM wave travels approximately at the speed of light,  $c = 3.0 \times 10^8 m/s$ . Hence, the time it takes for the signal to reflect off of a target and return to the antenna is given as:

$$\tau = \frac{2r}{c} \quad (11)$$

To calculate the Doppler frequency of a signal, the following equation is used.

$$f_D = \frac{2v}{\lambda} \quad (12)$$

Where  $\lambda = c/f_c$  is the wavelength of the waveform in meters, and  $v$  is the velocity profile of the target. With the ability to calculate the time delay and Doppler shift of the target, the receiver can find other properties of the target. The receiver can locate both the line-of-sight distance i.e. the range, and the orthogonal distance i.e. the cross-range, of a target.

### 4.3 The Linear FM Waveform

The most commonly used radar waveform is the linear frequency modulated (LFM) waveform. As the name suggests, its instantaneous frequency changes linearly as a function of time. This linearity can have either a positive or a negative slope. The instantaneous frequency at any given time is:

$$x(t) = t \quad (13)$$

Then, the LFM signal is given as:

$$s_{LFM}(t) = A \cos(2\pi K \int_0^t \lambda d\lambda) \quad (14)$$

One of the disadvantages of the LFM waveform is that it cannot be used for high-resolution radar imaging. A linear FM waveform is only able to extract the range information of a target. In addition, its ambiguity function yields a range-Doppler coupling which is not desirable for high-resolution imaging. In contrast, noise or noise-like waveforms yield a thumbtack ambiguity function that is desirable for high-resolution radar imaging.

## 4.4 The Chaos-Based FM Waveform

Chaos-based FM waveforms are generated using chaotic state variables. Chaotic waveforms are aperiodic with noise-like behavior, causing the signals that implement them to possess a high bandwidth. This is a desirable quality in generating high-resolution images as the range resolution is dependent on the bandwidth of the signal. Additionally, this is desirable for ECCM capabilities as a jammer concentrates its power in a narrow range of frequencies. Chaotic systems are also deterministic meaning that they are feasible to implement with electronic circuits [10]. There are various types of chaotic systems in both the continuous and discrete domains. For a continuous chaotic waveform, the system can be represented using nonlinear differential equations. Each differential equation, or state-variable, corresponds to a waveform where the amplitude of the waveform is a voltage as a function of time. A discrete map is given by iterative difference equations where the voltages are generated, not as a function of continuous time, but rather as a function of sampling intervals.

# 5 Preliminary Methodology

## 5.1 The Chaotic Systems

The chaotic systems used in this work are the Moore-Spiegel system, the Lorenz system, the ACT system, and the Rossler system. Each system is represented by three state variables  $x(t)$ ,  $y(t)$ , and  $z(t)$ , all of which are obtained by integrating nonlinear differential equations. They are continuous systems, as opposed to previously implemented discrete maps such as the Bernoulli, Tent, Logistic, and Quadratic maps. The Moore-Spiegel system is given as [14]:

$$\begin{aligned}\frac{dx}{dt} &= Cy \\ \frac{dy}{dt} &= Cz \\ \frac{dz}{dt} &= C(-z - (T - R + Rx^2)y - Tx)\end{aligned}\tag{15}$$

Where the parameters were given as  $T = 6$ ,  $R = 20$ . The Lorenz system is given as [14]:

$$\begin{aligned}\frac{dx}{dt} &= C\sigma(y-x) \\ \frac{dy}{dt} &= C(x(\rho-z)-y) \\ \frac{dz}{dt} &= C(xy-\beta z)\end{aligned}\tag{16}$$

Where the parameters,  $\sigma$ ,  $\rho$ , and  $\beta$  are equal to 10, 28 and 8/3. The ACT system is given as [14]:

$$\begin{aligned}\frac{dx}{dt} &= C\alpha(x-y) \\ \frac{dy}{dt} &= C(-4\alpha y+xz+\mu x^3) \\ \frac{dz}{dt} &= C(-\delta\alpha z+xy+\beta z^2)\end{aligned}\tag{17}$$

Where  $\alpha = 1.8$ ,  $\beta = -0.07$ ,  $\delta = 1.5$ , and  $\mu = 0.05$ . The Rossler system is given as [14]:

$$\begin{aligned}\frac{dx}{dt} &= C(-y-z) \\ \frac{dy}{dt} &= C(x+ay) \\ \frac{dz}{dt} &= C(b+z(x-c))\end{aligned}\tag{18}$$

Where  $a = 0.2$ ,  $b = 0.5$ , and  $c = 5.7$ .

The chaotic systems are sensitive to their initial conditions  $x(0)$ ,  $y(0)$ , and  $z(0)$ . If two FM waveforms are generated with the same system, but the initial condition is varied slightly among each waveform, the two waveforms will appear to be very different. Hence, correlation between these two generated FM waveforms will be very low. The initial conditions were provided by [14], and are shown in Table 1.

Multiple realizations of CBFM waveforms were generated by changing the initial conditions. These initial conditions were changed with a random number in the range of  $[-\frac{1}{1000}, \frac{1}{1000}]$ . These multiple realizations are necessary to conduct Monte-Carlo simulations to observe the statistical behavior of each waveform.

<b>Chaotic System</b>	<b>Initial Conditions</b>
Moore-Spiegel	$x = 0.1, y = 0, z = 0$
Lorenz	$x = -5.6599, y = -11.1608, z = 7.5402$
ACT	$x = 3.0191, y = 1.3046, z = 3.032$
Rosler	$x = -4.3758, y = -2.6917, z = 0.0194$

*Table 1: Initial Conditions for Generating Chaotic Waveforms*

## 5.2 Compression Factors

The compression factors, or  $C$ , in each set of equations, were significant in ensuring the chaotic state variables were all oscillating at a similar rate. The final values chosen are shown in Table 2. Modifying the compression factors is feasible using electronic hardware. Assuming the circuit for a chaotic waveform is constructed with an op-amp, the compression factor can be controlled by the capacitance of the circuit. As one decreases the value of the circuit's capacitance, one can increase the compression factor of the voltage waveform. With an increased compression factor, the oscillation of the waveform is increased.

<b>Chaotic System</b>	<b>Compression Factor</b>
Moore-Spiegel	$1.3 \times 10^7$
Lorenz	$5.0 \times 10^6$
ACT	$1.5 \times 10^7$
Rosler	$2.5 \times 10^7$

*Table 2: Finalized Compression Factors*

## 5.3 Generating the Transmitted Waveforms

For each of the systems, an FM signal was generated with the system's x-state variable. To avoid spectral aliasing, the x-state variables are first normalized to the range of  $[-1,1]$ . The amplitude  $A$  of each FM signal, represented by Equation (9), was set to 1V. The pulse width of each waveform was set to  $30 \mu s$ . The sampling time was considered to be  $1 ns$ . Figure 2 displays the instantaneous frequency for each of the transmitted signals.

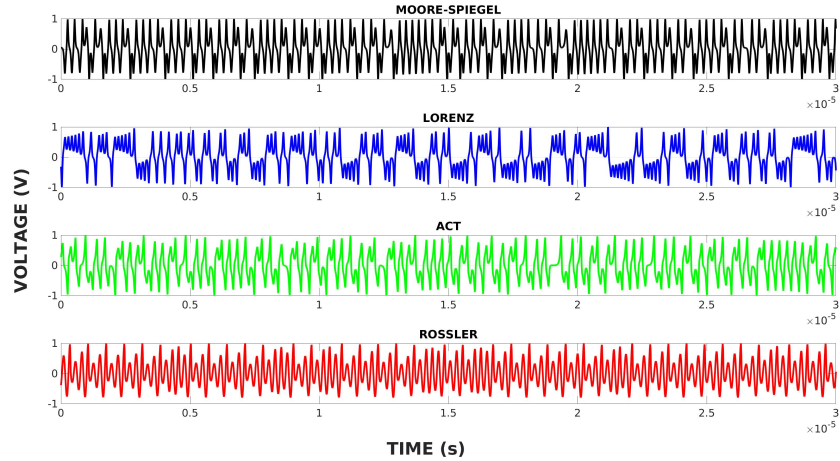


Figure 2: Voltage of  $x$ -state variables over time for each chaotic system

## 6 Characteristics of CBFM Waveforms

After generating transmitted FM waveforms using chaotic variables shown in Figure 2, we computed the power spectrums and autocorrelations of the CBFM waveforms.

### 6.1 The FM Waveforms in the Frequency Domain

The power spectrum is used to determine the FM waveforms' distribution of power in the frequency domain. It is calculated using the squared magnitude of the Fourier Transform of a waveform as given below:

$$S(f) = |F\{s(t)\}|^2 \quad (19)$$

A uniformly spread spectrum is desired for high-resolution imagery and ECCM capabilities. A wideband spectrum results in a sharp autocorrelation, which is necessary for high-resolution imaging. A wideband spectrum is also indicative of better ECCM capabilities because a jammer allocates all of its power within a narrow band of frequencies [16]. The power spectrums were calculated and averaged over 100 realizations where each realization has a slightly varied set of

initial conditions. After calculating each spectrum, its magnitude is normalized in the range of [0, 1]. The power spectrums of each chaotic system are shown in Figure 3.

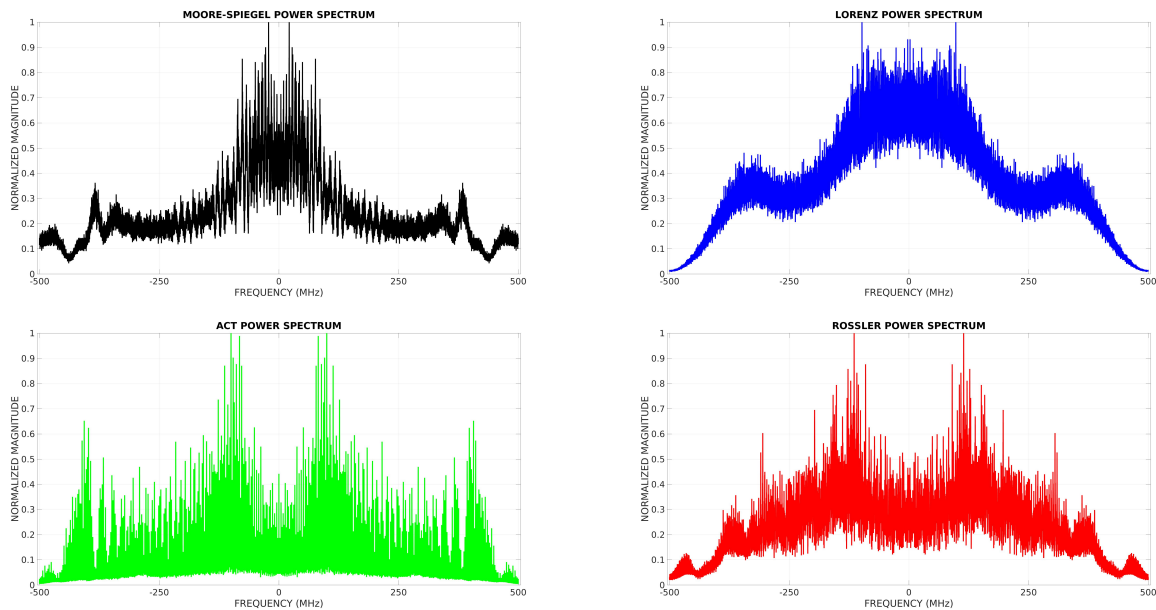


*Figure 3: Power Spectrums of the CBFM Signals over 100 Monte-Carlo Simulations*

A uniform distribution of power is shown in the spectrums of ACT and Rossler, so it is expected that they have better performance in terms of imaging and ECCM capabilities. The Lorenz system has most of its power concentrated near zero frequency and 300 MHz. This indicates it would not perform as well as the previous two systems. The Moore-Spiegel system has its power mainly concentrated at DC, so it is expected to have the least performance compared to all other systems.

## 6.2 Autocorrelations

Cross-correlation is used to correlate the transmitted waveform with the received waveform. A special case of cross-correlation is autocorrelation that is used to correlate the signal by itself. It is used to test the capability of the transmitted waveform in detecting the target and to signify the high-resolution capability of the transmitted waveform. It is mathematically defined as (20):

$$R_{ss}(\tau) = \int_{-\infty}^{+\infty} s(t)s(t - \tau)dt \quad (20)$$

The result of the autocorrelation is a peak, or a spike in magnitude, at some time delay  $\tau$ . This is a fundamental component of how the radar processes the received signal because the receiver uses a series of correlations to determine the time delay associated with the target.

Ideally, there should only be one peak at the time delay  $\tau$  of the waveform, and the autocorrelation would resemble a Dirac delta function. However, this is not practically possible. Instead a mainlobe peak at  $\tau$  is surrounded by sidelobe peaks. It is a goal in radar design to reduce the levels of the sidelobes. For high-resolution imaging, the sidelobes must be below the level of -13.33 dB. This is because the typical radar waveform employs linear FM, and the spectrum of a linear FM waveform is approximated to have a rectangular shape. As the autocorrelation is the inverse Fourier transform of the spectrum, the autocorrelation for an LFM waveform is approximated to be a *sinc* function [12]. The first sidelobe of a *sinc* function occurs at  $t = \frac{3\pi}{2}$ , and  $sinc_{dB}(\frac{3\pi}{2}) = -13.33$  dB. Figure 4 displays that each of the systems sidelobes are below -13.33 dB.

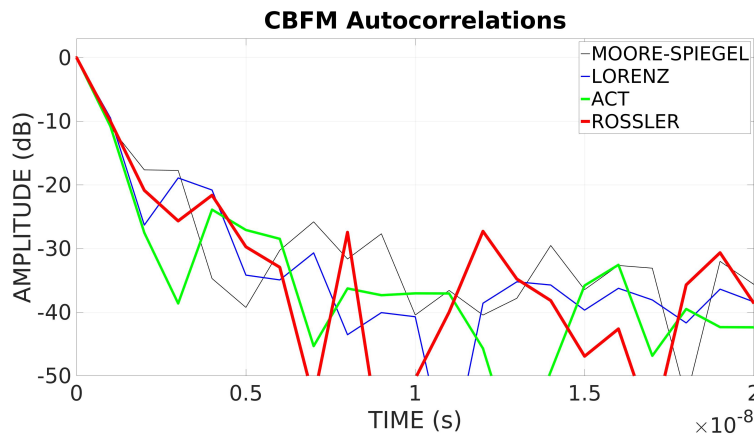


Figure 4: Sidelobe levels from Autocorrelations of CBFM Waveforms

As expected based on the power spectrum, the waveform that used Moore-Spiegel had the highest sidelobe level and the ACT system had the lowest sidelobes.

Additionally, the autocorrelation determines the range resolution of the image generated by the radar. Range resolution is an ability to determine two closely spaced targets. Range resolution of a monotone signal depends on the pulse width, whereas for the modulated signal it depends on the

bandwidth of the signal [16]. Range resolution is calculated as [12]:

$$\Delta r = \frac{c}{2BW} \quad (21)$$

Where  $c$  is the speed of light, and  $BW$  is the bandwidth of the signal. Consequently, a wideband signal can have a high range resolution.

An estimate of the signal's bandwidth can also be found using autocorrelation. For a modulated signal, the bandwidth is obtained as the inverse of the autocorrelation mainlobe width. The mainlobe width of the autocorrelations at -3 dB for each of the CBFM waveforms is shown in Figure 5.

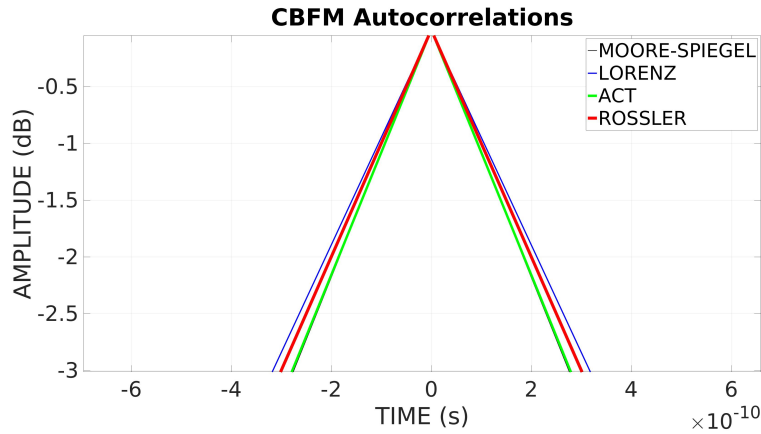


Figure 5: Mainlobes of waveforms at -3dB

The time lag for all of the waveforms was roughly 0.3 ns on each side, or 0.6 ns in total. The bandwidth is the inverse to the time lag, or  $\frac{1}{\Delta t} = \frac{1}{0.6ns} = 1.5$  GHz. With a signal bandwidth of 1.5 GHz, the range resolution is 0.1 m.

## 7 Implementation of a Smart Jammer

To examine the ECCM capabilities of each waveform, a smart jammer based on [8] was implemented. This type of jammer demodulates the transmitted signal using the signal's In Phase and

Quadrature components to acquire the signal's instantaneous frequency. A block diagram for this demodulation technique, I/Q demodulation, is shown in Figure 6.

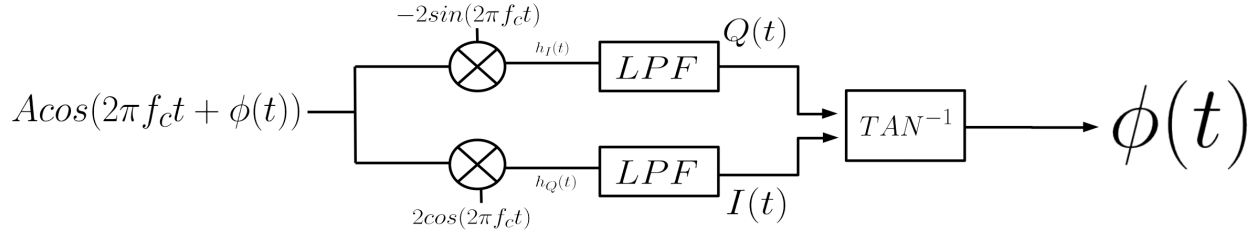


Figure 6: I/Q Detector Block Diagram

The  $h_I(t)$  and  $h_Q(t)$  components are derived as:

$$\begin{aligned}
 h_I(t) &= r(t) \times 2\cos(2\pi f_c t) \\
 &= A\cos(2\pi f_c t + \phi(t)) \times 2\cos(2\pi f_c t) \\
 &= \frac{1}{2}[2A\cos(2\pi f_c t + \phi(t) + 2\pi f_c t) + 2A\cos(2\pi f_c t + \phi(t) - 2\pi f_c t)] \\
 &= A\cos(2(2\pi f_c t) + \phi(t)) + A\cos(\phi(t))
 \end{aligned} \tag{22}$$

$$\begin{aligned}
 h_Q(t) &= r(t) \times -2\sin(2\pi f_c t) \\
 &= A\cos(2\pi f_c t + \phi(t)) \times -2\sin(2\pi f_c t) \\
 &= \frac{1}{2}[-2A\sin(2\pi f_c t + \phi(t) + 2\pi f_c t) + 2A\sin(2\pi f_c t + \phi(t) - 2\pi f_c t)] \\
 &= -A\sin(2(2\pi f_c t) + \phi(t)) + A\sin(\phi(t))
 \end{aligned} \tag{23}$$

The resulting spectral representation of the  $h_I(t)$  and  $h_Q(t)$  waveforms display frequency components at  $+2f_c$ ,  $-2f_c$ , and the original frequency centered at  $0f_c$ . The  $h_I(t)$  and  $h_Q(t)$  frequency spectrums for the ACT system is shown in Figure 7. The blue plot indicates the  $h_I(t)$  component and the black plot indicates the  $h_Q(t)$  component.

In this simulation, the carrier frequency was 200 MHz so there were frequency components at 400 MHz, -400 MHz, and 0 MHz. To remove the components located at 400 MHz and -400 MHz, a fifth order Butterworth low pass filter with a cutoff frequency of 400 MHz was implemented. The resulting spectrums of the  $I(t)$  and  $Q(t)$  components are shown in Figure 8. The blue plot indicates

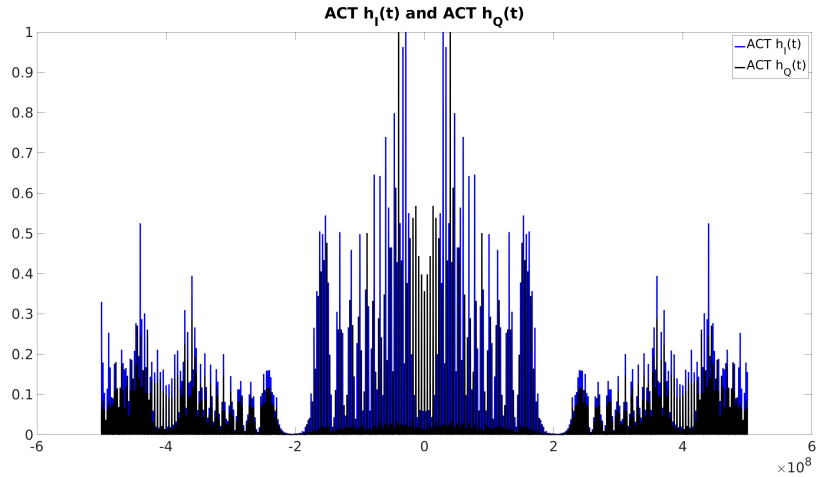


Figure 7: Jammer Extracted  $h_I(t)$  and  $h_Q(t)$  Components of ACT System

the  $I(t)$  component and the black plot indicates the  $Q(t)$  component.

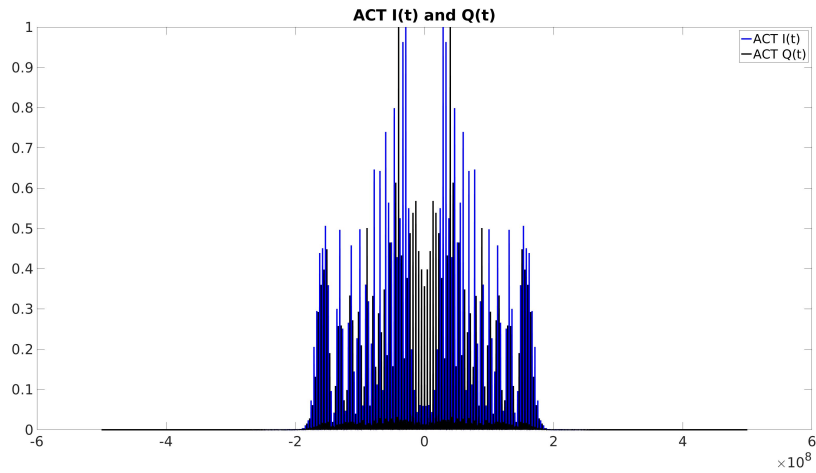


Figure 8: Jammer Extracted  $I(t)$  and  $Q(t)$  Components of ACT System

After filtering, the resulting  $I(t)$  and  $Q(t)$  waveforms represent  $\cos(\phi(t))$  and  $\sin(\phi(t))$  respectively. By taking the arctangent of these two waveforms, the jammer can extract an estimate of the instantaneous phase as shown in Equation (24).

$$\begin{aligned}
\phi(t) &= \tan^{-1} \left( \frac{Q(t)}{I(t)} \right) \\
\phi(t) &= \tan^{-1} \left( \frac{\sin(\phi(t))}{\cos(\phi(t))} \right) \\
\phi(t) &= \tan^{-1} (\tan(\phi(t)))
\end{aligned} \tag{24}$$

Then, an estimate of the instantaneous frequency was found from the phase with Equation (5). With an estimate of the instantaneous frequency, the jammer modulates the instantaneous frequency and transmits an FM waveform. If the recovered instantaneous frequency is accurate in comparison to the actual instantaneous frequency of the transmitted signal, the radar perceives the signal to be reflected off of some target thereby creating a false alarm. The radar has no way of discriminating between an actual echo from a target and a waveform originating from the jammer. A radar could avoid the effect of a jammer if the difference between the jammer's instantaneous frequency and the actual instantaneous is great. To observe if the CBFM waveforms could avoid the jammer's ability to recover the instantaneous frequency, each CBFM waveform was tested under the smart jamming model. The root mean squared error was taken between the actual instantaneous frequency and the jammer's recovered instantaneous frequency over various iterations of testing. In each iteration, the bandwidth of each system was increased by increasing the modulation index of the signal. The first minimum bandwidth for each system was around 15 MHz, and the final bandwidth tested was around 3 GHz. For each bandwidth, Monte-Carlo simulations were conducted, and the results were averaged over 10 trials.

The RMSE results between the jammer's recovered instantaneous frequency and the actual instantaneous frequency of the transmitted signal are shown in Figure 9.

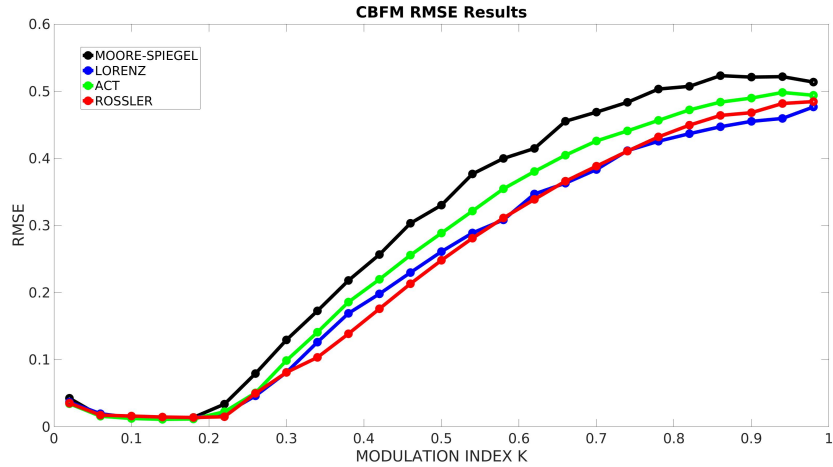


Figure 9: RMSE Between Actual and Recovered Instantaneous Frequency

When the modulation index is in the range from 0.01 to 0.2, the bandwidth is in the range of 15 MHz to 350 MHz and the jammer is able to recover the signal’s frequency with little error. When the modulation index is increased to 0.5, or the bandwidth is approximately 1.5 GHz, the recovered frequency began to differ significantly from the actual frequency. As the bandwidth increased beyond this point, the level of error continues to increase. The difference in actual against recovered instantaneous frequency is shown in Figure 10.

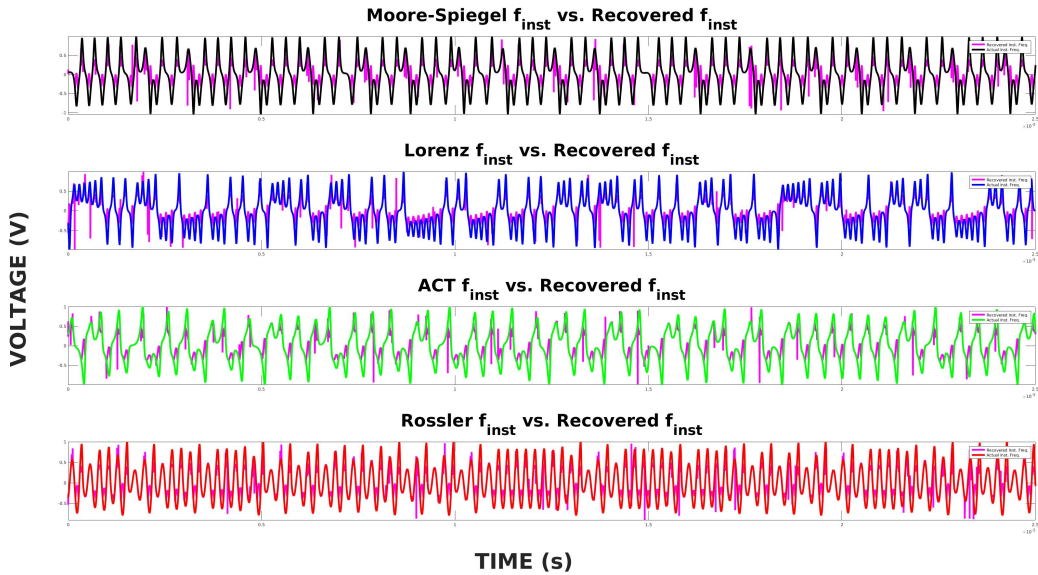


Figure 10: Actual and Recovered Instantaneous Frequency at K=0.5

Though all of the systems were able to counteract the jammer, the Moore-Spiegel system had the greatest level of error compared to the rest of the systems. The reason for this is currently under investigation as the Moore-Spiegel CBFM was expected to perform worse than the other systems.

## 8 Implementation of High-Resolution Imaging

A complex target was then considered to demonstrate the image resolution produced by the chaotic waveforms. Each point on the target was considered as a hotspot, where there is a time delay and Doppler shift corresponding to each point. The received signal for the complex target is a summation of reflections from all of the hotspots representing the contour of the target. The target chosen was a full scale 73x65 meter Boeing 737 airplane. The dimensions of the target are shown in Figure 11.

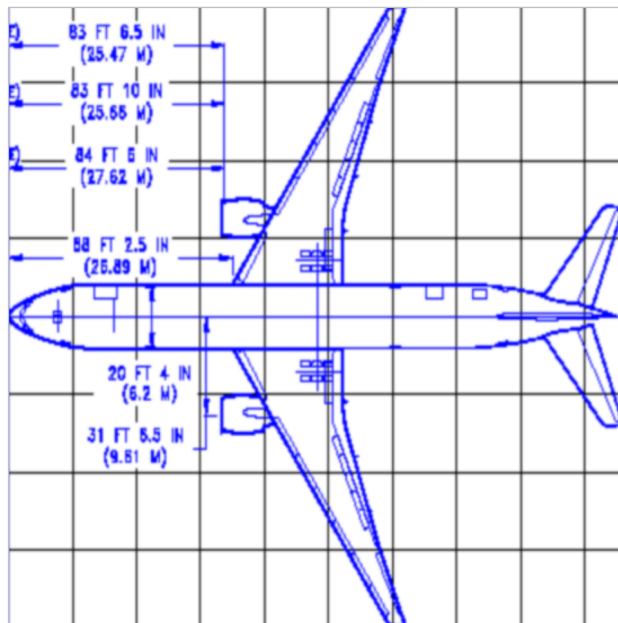


Figure 11: X and Y Dimensions of Complex Target

## 8.1 Ambiguity Functions

The ambiguity function was implemented to calculate the time delay and the Doppler frequency shift at the origin  $\tau = 0$  s and  $f_D = 0$  Hz [15]. The ambiguity function employs a series of correlations between the transmitted signal (reference) and the received signal, which is a delayed and Doppler-shifted replica of the transmitted signal. This process is also called matched filtering. When the Doppler frequency of the reference signal matches the Doppler frequency of the received signal, a peak occurs at the corresponding time delay and Doppler shift. The ambiguity function is given as:

$$\chi(\tau, f_D) = \left| \int_{-\infty}^{\infty} s(t)s(t-\tau)e^{j2\pi f_D t} dt \right|^2 \quad (25)$$

The ideal ambiguity function should take on the shape of a Dirac delta function at the origin [9]. Because the Dirac delta function is not practically possible to achieve, the ambiguity function of a thumbtack shape is desirable.

The results of the ambiguity function for each system are shown in Figure 12. The magnitude value of the mainlobe peak is 0 dB, which occurs at the origin. The sidelobes surrounding the mainlobe is below -13.33 dB. These results indicate that each chaotic system is capable of high-resolution imaging.

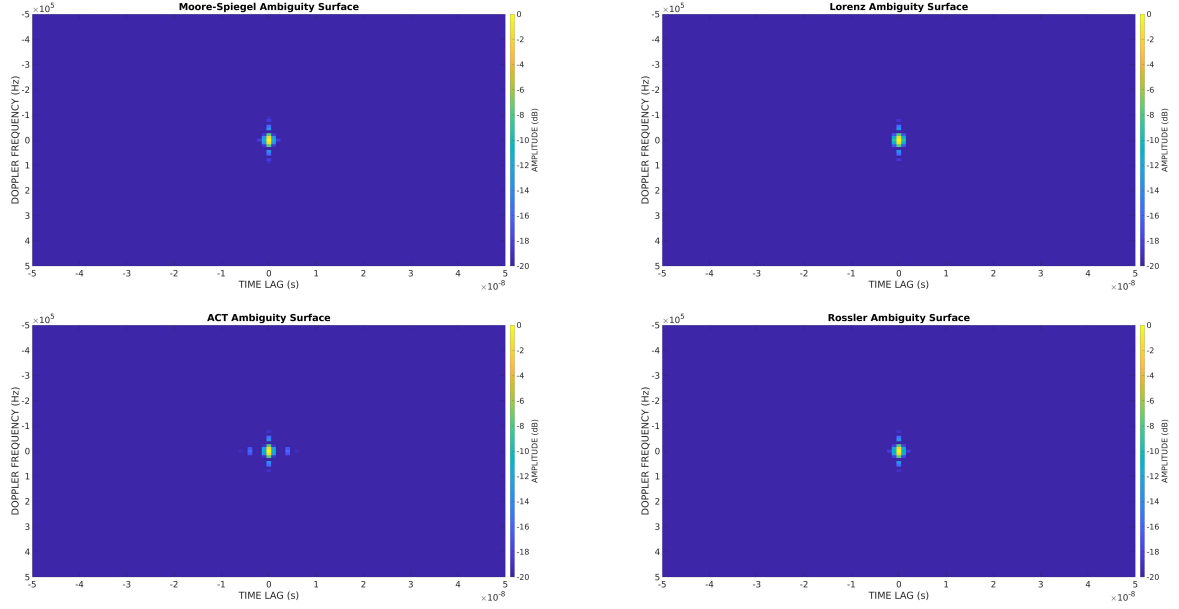


Figure 12: Results of the Ambiguity Function with Time  $\tau = 0$  s and  $f_D = 0$  Hz

## 8.2 Signature Analysis

To implement signature analysis, first, a transmitted waveform was generated with a pulse width of  $30\mu\text{s}$  and a sampling time of  $1\text{ ns}$ . The profile of the airplane was then set up by converting the X and Y coordinates of 23 hotspots in Figure 11 to their respective time delays and Doppler shifts. The airplane was assumed to be 1 km away from the radar. The additional line-of-sight distances of each hotspot were found to calculate the hotspot's delay using Equation (11). The velocity profile of each hotspot was calculated to estimate the Doppler frequency using Equation (12). The velocity profile of the target is given by

$$v = \Omega r_c \quad (26)$$

Where  $r_c$  is the cross-range, or orthogonal distance from the target to the radar.  $\Omega$  is the target's total angular speed in rad/sec given by:

$$\Omega = \frac{\Delta\theta}{T_{int}} \quad (27)$$

Where  $T_{int}$  is the integration time or pulse width of the signal, and  $\Delta\theta$  is the target's total angular rotation given by:

$$\Delta\theta = \frac{BW}{f_c} \quad (28)$$

The received waveform can now be modelled as the sum of reflections from each hotspot with the corresponding time delay and Doppler shift. The received waveform is given as:

$$r(t) = \sum_{k=1}^N s(t - \tau_k) e^{j(2\pi f_c t + 2\pi f_{D_k} t)} \quad (29)$$

Where N represents the total number of hotspots.

The received signal is now processed to extract the range and cross range information of the target. First, a matched filter bank was implemented such that each filter has a response identical to the reference but tuned to a particular Doppler frequency. For the airplane as a target, the range of these Doppler frequencies was considered to be  $-100f_D$  to  $100f_D$  where  $f_D = \frac{1}{T_{int}} = \frac{1}{30\mu s} = 33$  kHz. After the received signal is driven through these matched filters, a peak is observed whenever the reference signal's Doppler frequency is equivalent to one of the received signal's Doppler frequencies. The peak is displayed at the delay and the Doppler frequency of that hotspot. After driving the reference signal through each filter, the image of the target is generated. A block diagram of the signature analysis is shown in Figure 13. In the Figure,  $r(t)$  represents the received signal, and each  $\hat{f}_D$  represents the  $N$ th reference signal tuned at their individual Doppler frequency  $\hat{f}_{D_k}$ . Each row in the resulting signature analysis is given by a correlation between the received signal and the reference signal. For signature analysis, 10 Monte-Carlo realizations were conducted for each chaotic system.

The signature analysis was converted to the Decibel scale using  $10 \times \log_{10}(\text{Signature Analysis})$ . The noise floor was set at -20dB.

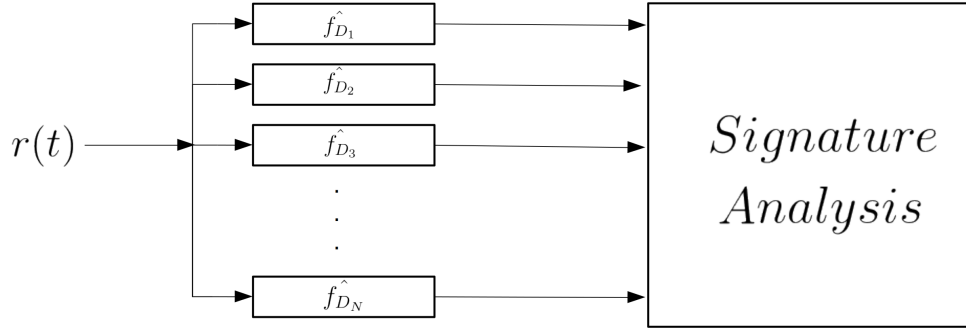


Figure 13: Block Diagram of Signature Analysis

### 8.3 Signature Analysis with Noise

In real time scenarios, the received signal is corrupted with noise. The actual received waveform is given as:

$$r(t) = s(t - \tau)e^{j2\pi f_D t} + \eta(0, \sigma^2) \quad (30)$$

Where  $\eta(0, \sigma^2)$  is additive white Gaussian noise with a mean of 0 and variance  $\sigma^2$ . We illustrate the effects of noise on high-resolution capability of the radar. To implement this, the power of the transmitted signal and the power of noise were derived. As the amplitude of an FM signal is a constant with  $A$  volts, its average power is given as:

$$P_{avg} = \frac{A^2}{2} \quad (31)$$

As  $A$  was set to 1V, the power of the transmitted signal was 0.5 W.

Because the noise was assumed to be additive white Gaussian noise, its power is given as the expected value of the random variable. The derivation for the expected value of the Gaussian noise is given as:

$$\begin{aligned}
P_{noise} = E[X^2] &= \int_{-\infty}^{+\infty} f_x(x) dx \\
&= \int_{-\infty}^{+\infty} x^2 \frac{1}{\sqrt{2\pi\sigma^2}} e^{\frac{-x^2}{2\sigma^2}} dx \\
&= \frac{1}{\sqrt{2\pi\sigma^2}} \int_{-\infty}^{+\infty} x^2 e^{\frac{-x^2}{2\sigma^2}} dx \\
&= \frac{1}{\sqrt{2\pi\sigma^2}} \left[ x(-\sigma^2 e^{\frac{-x^2}{2\sigma^2}} - \int -\sigma^2 e^{\frac{-x^2}{2\sigma^2}} dx) \right] \\
&= \frac{-\sigma^2}{\sqrt{2\pi\sigma^2}} \left[ x e^{\frac{-x^2}{2\sigma^2}} \right] \Big|_{-\infty}^{+\infty} + \frac{\sigma^2}{\sqrt{2\pi\sigma^2}} \int e^{\frac{-x^2}{2\sigma^2}} dx \\
&= \frac{\sigma^2}{\sqrt{2\pi\sigma^2}} \left[ 2 \int e^{\frac{-x^2}{2\sigma^2}} dx \right] \\
&= \frac{\sigma^2}{\sqrt{2\pi\sigma^2}} (\sqrt{2\pi\sigma^2}) \\
&= \sigma^2
\end{aligned} \tag{32}$$

Thus, the power of the noise signal was a function of its variance,  $\sigma^2$ . Various noise levels were simulated by modifying the variance of an additive white Gaussian noise waveform. To find the variance needed for a specific SNR level, the standard deviation, or square root of the variance, was expressed as a function of the power of the signal and the desired SNR level. This derivation is shown in Equation (33).

$$\begin{aligned}
10 \log_{10} \frac{P_{avg}}{\sigma^2} &= SNR_{dB} \\
\log_{10} \frac{P_{avg}}{\sigma^2} &= \frac{SNR_{dB}}{10} \\
\frac{P_{avg}}{\sigma^2} &= 10^{\frac{SNR_{dB}}{10}} \\
\sigma^2 &= \frac{P_{avg}}{10^{\frac{SNR_{dB}}{10}}} \\
\sigma &= \sqrt{\frac{P_{avg}}{10^{\frac{SNR_{dB}}{10}}}}
\end{aligned} \tag{33}$$

The SNRs that were used in imaging were: -5 dB, -10 dB, -15 dB, -20 dB.

## 8.4 Entropy Analysis

Entropy analysis was used to measure the amount of information lost in signature analysis with different levels of noise added on to the received signal. Ideally, each pixel of the signature analysis should be a 0 or a +1 depending on the presence of a hotspot. However, there is always additional sidelobes that occur due to the presence of noise and any energy spillover in the sidelobes of the correlations. Thus, entropy of the image is calculated to quantify the effect of noise and energy spillover for each radar waveform in signature analysis. Entropy is calculated by:

$$H = \frac{-1}{mn} \sum_{i=1}^m \sum_{j=1}^n I(i, j) \log_2(I(i, j)) \quad (34)$$

Where  $I$  is the image,  $i$  and  $j$  represent each row and column iterated over the total  $m$  rows and  $n$  columns of the image. The resulting entropy should theoretically be at 0 if the signature analysis was perfectly discretized at values of 0's and 1's. However, due to the impacting conditions mentioned previously, this is not possible. By finding the entropy for each system, it is possible to determine which of the systems were least affected by noise and had the least amount of energy spillover. For each system, entropy is calculated over SNR levels from 0 dB to -40 dB, and were averaged over 5 iterations.

## 9 Performance Estimates and Results

### 9.1 Signature Analysis Results

The resulting signature analysis for each system is given in Figure 14.

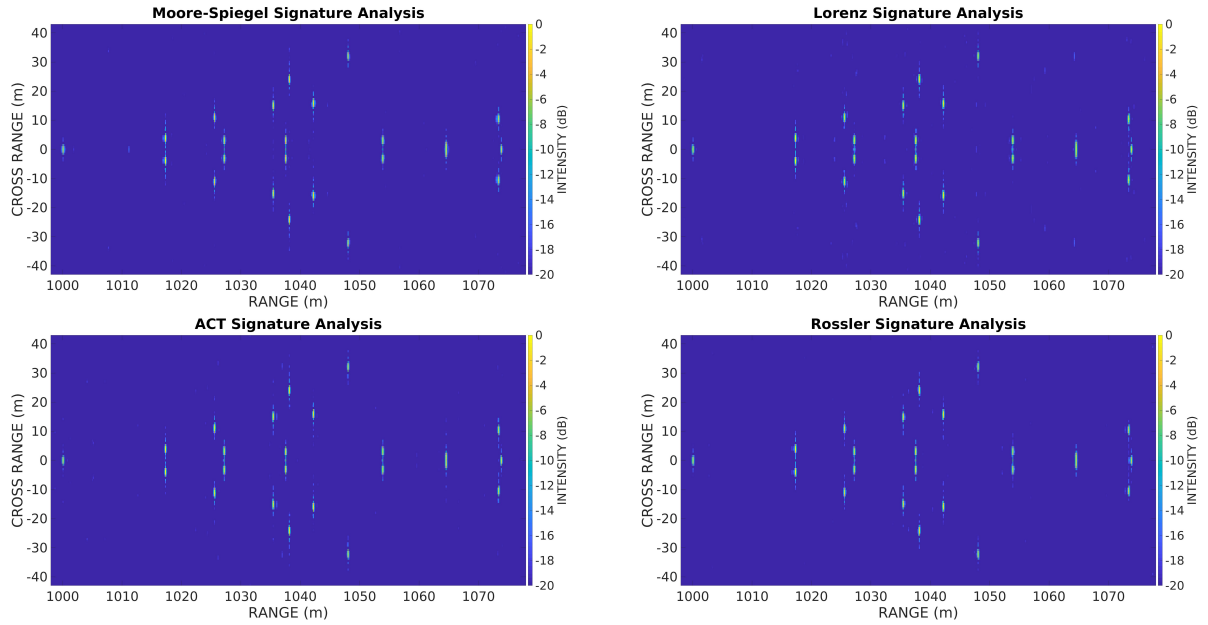


*Figure 14: Signature Analysis Results with SNR = 0dB*

Each system possesses high-resolution imaging capabilities. All of the hotspots were distinguishable from each other, and none of the hotspots were overlapping. Also, the range resolution observed met the expected value of 0.1m. The signature analysis using the ACT system over different SNRs is shown in Figure 15.

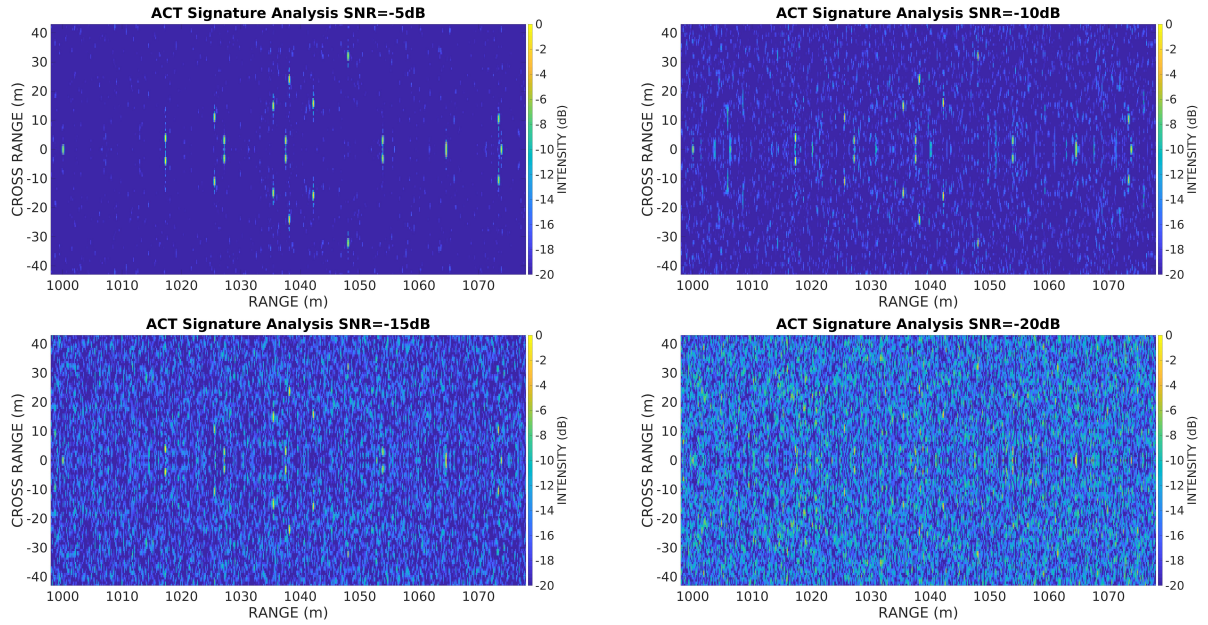


Figure 15: ACT Signature Analysis with SNR = -5dB, -10dB, -15dB, -20dB

As the power of the noise was increased, the appearance of the hotspots became progressively less visible. Figure 15 shows that each hotspot is still visible when the SNR is -15 dB. After this point, the hotspots became indistinguishable from the noise.

## 9.2 Entropy Analysis Results

The result of the entropy is shown in Figure 16.

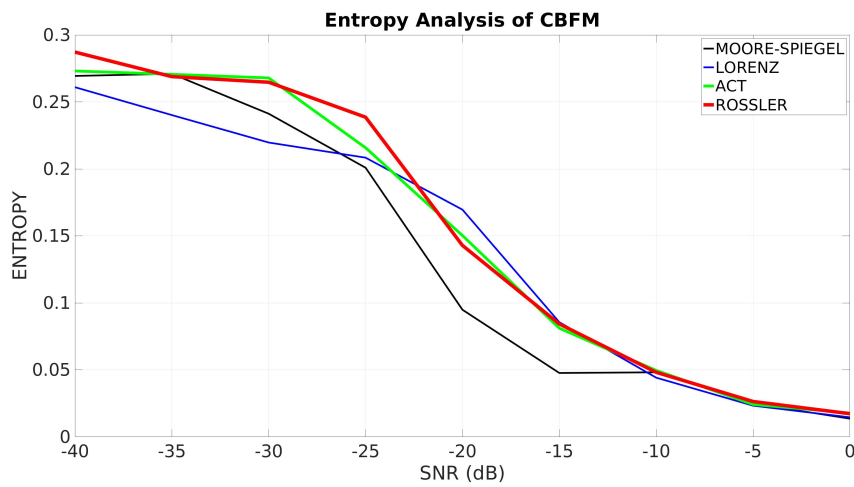


Figure 16: Entropy Analysis of Waveforms at SNR levels from -40 dB to 0dB

All of the systems demonstrated similar entropy values over various SNR levels, and each approaches a greater level of entropy as the SNR decreases. The Moore-Spiegel system maintained the least amount of entropy throughout the trials. At SNR = -15 dB, the Moore-Spiegel system had an entropy level of around 0.05, while the other systems had entropy levels closer to 0.08. At SNR = -20 dB, the Moore-Spiegel system had an entropy level of around 0.1, while the other systems had entropy levels around 0.15. When the SNR was further decreased, all of the systems had entropy levels approaching 0.3.

## **10 Discussion, Conclusion, and Recommendations**

Four chaotic systems, the Moore-Spiegel system, the Lorenz system, the ACT system, and the Rossler system were introduced in a monostatic radar setting. Various tests were used to determine the ECCM capabilities and the high-resolution imaging capabilities of each system when implemented in a monostatic radar.

The power spectrums and autocorrelations were computed for each FM waveform to analyze the high-resolution capabilities of each chaos-based waveform. Then, a smart jammer was implemented to extract the instantaneous frequency of the transmitted waveforms. It was found that by increasing the bandwidth to 1.5 GHz and higher, the instantaneous frequency of the transmitted signal may not be accurately recovered, and all of the chaotic systems were able to counteract the jammer. The ambiguity function was computed to assess the high-resolution imaging capability of a single target, and signature analysis was considered to observe the high-resolution imaging capability for a complex airplane target. It was found that each of the chaotic systems were able to produce high-resolution images of the target, and the range resolution was found to be 0.1m. By adding higher levels of noise to the image, the quality of the signature analysis decreased. When the SNR approached -15 dB and beyond, the hotspots of the targets were indistinguishable from the noise. After conducting entropy analysis for each of the systems at SNR levels of 0 to -40 dB, the Moore-Spiegel system displayed the least amount of entropy in the -15 dB to -20 dB range.

I would recommend for future research to run more Monte-Carlo simulations to get a better understanding of the performance of each chaotic system in a radar. As it was unexpected for the Moore-Spiegel system to have the least amount of entropy in signature analysis, it could potentially be due to the lack of large-scale data acquired for each system. If not, it would be of importance to identify the cause of Moore-Spiegel having the best performance.

## **10.1 Lessons Learned**

Many lessons were learned throughout this process. The first lesson was to understand the full context of the project and any previous work done. Many problems that arise could have already been encountered and solved in previous research. Additionally, it is not as straightforward to convert a theoretical concept to a computer program. There may be much more work involved when translating something to code than it first seems. Also, it is essential to refer to old notes. Newer concepts may seem unfamiliar at first, but the context for the new concept may have been developed in previous notes. Lastly, it is essential to keep code organized, commented, and reusable. When working on a program, it is important that the code still makes sense when editing it a few days later.

## 11 References

- [1] Ali Ashtari et al. “Radar signal design using chaotic signals”. In: *2007 International Waveform Diversity and Design Conference*. IEEE. 2007, pp. 353–357.
- [2] Andreas Bauer. “Chaotic signals for CW-ranging systems. A baseband system model for distance and bearing estimation”. In: *ISCAS’98. Proceedings of the 1998 IEEE International Symposium on Circuits and Systems (Cat. No. 98CH36187)*. Vol. 3. IEEE. 1998, pp. 275–278.
- [3] Andreas Bauer. “Utilisation of chaotic signals for radar and sonar purposes”. In: *Norsig*. Vol. 96. 1996, pp. 33–36.
- [4] *Electromagnetic fields and public health: radars and human health*. Aug. 2016. URL: <https://www.who.int/peh-emf/publications/facts/fs226/en/>.
- [5] Benjamin C Flores, Chandra S Pappu, and Berenice Verdin. “Generation of FM signals with quasi-chirp behavior using three-dimensional chaotic flows”. In: *Radar Sensor Technology XV*. Vol. 8021. International Society for Optics and Photonics. 2011, p. 80210V.
- [6] Benjamin C Flores, Emmanuel A Solis, and Gabriel Thomas. “Assessment of chaos-based FM signals for range–Doppler imaging”. In: *IEE Proceedings-Radar, Sonar and Navigation* 150.4 (2003), pp. 313–322.
- [7] Benjamin C Flores, Emmanuel A Solis, and Gabriel Thomas. “Chaotic signals for wide-band radar imaging”. In: *Algorithms for Synthetic Aperture Radar Imagery IX*. Vol. 4727. International Society for Optics and Photonics. 2002, pp. 100–111.
- [8] Dmitriy S Garmatyuk and Ram M Narayanan. “ECCM capabilities of an ultrawideband bandlimited random noise imaging radar”. In: *IEEE Transactions on Aerospace and Electronic Systems* 38.4 (2002), pp. 1243–1255.
- [9] Jiann-Ching Guey and Mark R Bell. “Diversity waveform sets for delay-Doppler imaging”. In: *IEEE Transactions on Information Theory* 44.4 (1998), pp. 1504–1522.
- [10] SA Harman, AJ Fenwick, and C Williams. “Chaotic signals in radar?” In: *2006 European Radar Conference*. IEEE. 2006, pp. 49–52.
- [11] Bhagwandas Pannalal Lathi. *Modern Digital and Analog Communication Systems 3e Osece*. Oxford University Press, Inc., 1998.
- [12] Bassem R Mahafza. *Radar systems analysis and design using MATLAB*. Chapman and Hall/CRC, 2005.
- [13] Mark A Richards. *Fundamentals of radar signal processing*. Tata McGraw-Hill Education, 2005.
- [14] Julien Clinton Sprott and Julien C Sprott. *Chaos and time-series analysis*. Vol. 69. Citeseer, 2003.
- [15] T Tsao et al. “Ambiguity function for a bistatic radar”. In: *IEEE Transactions on Aerospace and Electronic Systems* 33.3 (1997), pp. 1041–1051.
- [16] Donald R Wehner. “High Resolution Radar, Artech House”. In: *Inc., Norwood, MA* (1987).
- [17] Nicholas J Willis. *Bistatic radar*. Vol. 2. SciTech Publishing, 2005.